Diagonally Inverted Lower-Upper Factored Implicit Multigrid Scheme for the Three-Dimensional Navier-Stokes Equations

Jeffrey W. Yokota*
Sverdrup Technology, Inc., NASA Lewis Research Center Group, Cleveland, Ohio 44135

A diagonally inverted, lower-upper, approximately factored, implicit multigrid algorithm is developed to calculate three-dimensional compressible viscous flows. This scheme solves the full Reynolds-averaged Navier-Stokes equations with a $k-\varepsilon$ model of turbulence. The flow equations are solved within the framework of the multigrid method using a four grid level W-cycle, while the $k-\varepsilon$ equations are solved only on the finest grid and uncoupled from the flow calculations. This treatment proves to be an efficient method for calculating three-dimensional compressible viscous flows.

Introduction

As the availability of larger and more powerful computers increases, so will the attention being directed towards computing complex three-dimensional (3-D) compressible viscous flows. At present the most successful approach has been to solve the thin-layer Navier-Stokes equations with an algebraic turbulence model. Most notable has been the work of Pulliam and Steger[1] and their highly successful ARC codes.

Attempts to produce efficient numerical schemes for the calculation of compressible viscous flows have led to the diagonalized alternating direction input (ADI) scheme of Chaussee and Pulliam[2] and more recently to the multigrid Runge-Kutta scheme of Jayaram and Jameson.[3] As emphasis increasingly focuses upon calculating complex three-dimensional flows, the need to efficiently solve numerically the Reynolds-averaged Navier-Stokes equations is correspondingly apparent.

The present work deals with the development of a multigrid scheme for the numerical solution of the Reynolds-averaged Navier-Stokes equations and the two equation $k-\varepsilon$ turbulence model. The Reynolds-averaged Navier-Stokes equations, which for mathematical closure requires the modeling of the Reynolds stress tensor, are solved by the diagonally inverted lower-upper (LU) implicit multigrid scheme developed by Yokota, Caughey, and Chima.[4] A Boussinesq eddy-viscosity formulation is used to model the Reynolds stress term, where the turbulent viscosities are calculated from a standard high-Reynolds-number $k-\varepsilon$ model.

Analysis

The three-dimensional Reynolds-averaged Navier-Stokes equations, with the Boussinesq eddy-viscosity formulation, are written in divergence form and then transformed from the Cartesian coordinate system (x,y,z) to the generalized system (ξ,η,ζ). The Jacobians of the coordinate transformation are:

$$J=\begin{pmatrix} x_\xi & x_\eta & x_\zeta \\ y_\xi & y_\eta & y_\zeta \\ z_\xi & z_\eta & z_\zeta \end{pmatrix}$$

$$J^{-1}=\begin{pmatrix} \xi_x & \xi_y & \xi_z \\ \eta_x & \eta_y & \eta_z \\ \zeta_x & \zeta_y & \zeta_z \end{pmatrix}$$

$$=\frac{1}{D}\begin{pmatrix} y_\eta z_\zeta - y_\zeta z_\eta & x_\xi z_\eta - x_\eta z_\zeta & x_\eta y_\zeta - x_\zeta y_\eta \\ y_\zeta z_\xi - y_\xi z_\zeta & x_\xi z_\zeta - x_\zeta z_\xi & x_\zeta y_\xi - x_\xi y_\zeta \\ y_\xi z_\eta - y_\eta z_\xi & x_\eta z_\xi - x_\xi z_\eta & x_\xi y_\eta - x_\eta y_\xi \end{pmatrix}$$

where D is the determinant of the matrix J, and the contravariant velocity components $(U,V,W)^T=J^{-1}(u,v,w)^T$ are derived from the Cartesian velocity components (u,v,w). The transformed flow equations can be written:

$$\frac{\partial \boldsymbol{W}}{\partial t}+\frac{\partial \boldsymbol{F}}{\partial \xi}+\frac{\partial \boldsymbol{G}}{\partial \eta}+\frac{\partial \boldsymbol{H}}{\partial \zeta}=\frac{\partial \boldsymbol{F}_v}{\partial \xi}+\frac{\partial \boldsymbol{G}_v}{\partial \eta}+\frac{\partial \boldsymbol{H}_v}{\partial \zeta} \tag{1}$$

with

$$\boldsymbol{W}=\begin{bmatrix} \rho D \\ \rho Du \\ \rho Dv \\ \rho Dw \\ DE \end{bmatrix} \quad \boldsymbol{F}=\begin{bmatrix} \rho DU \\ \rho DUu+PD\xi_x \\ \rho DUv+PD\xi_y \\ \rho DUw+PD\xi_z \\ DU(E+P) \end{bmatrix}$$

$$\boldsymbol{G}=\begin{bmatrix} \rho DV \\ \rho DVu+PD\eta_x \\ \rho DVv+PD\eta_y \\ \rho DVw+PD\eta_z \\ DV(E+P) \end{bmatrix} \quad \boldsymbol{H}=\begin{bmatrix} \rho DW \\ \rho DWu+PD\zeta_x \\ \rho DWv+PD\zeta_y \\ \rho DWw+PD\zeta_z \\ DW(E+P) \end{bmatrix}$$

Received April 17, 1989; revision received Sept. 29, 1989.

*Senior Research Engineer. Member AIAA.

$$\boldsymbol{F}_v = \begin{bmatrix} f_{v_1} \\ f_{v_2} \\ f_{v_3} \\ f_{v_4} \\ f_{v_5} \end{bmatrix} = \begin{bmatrix} 0 \\ D\xi_x\tau_{xx} + D\xi_y\tau_{xy} + D\xi_z\tau_{xz} \\ D\xi_x\tau_{xy} + D\xi_y\tau_{yy} + D\xi_z\tau_{yz} \\ D\xi_x\tau_{xz} + D\xi_y\tau_{yz} + D\xi_z\tau_{zz} \\ uf_{v_2} + vf_{v_3} + wf_{v_4} + \dfrac{\gamma}{\gamma-1}\tilde{\mu}_e\left(c_1\dfrac{\partial T}{\partial\xi} + c_2\dfrac{\partial T}{\partial\eta} + c_3\dfrac{\partial T}{\partial\zeta}\right) \end{bmatrix}$$

$$\boldsymbol{G}_v = \begin{bmatrix} g_{v_1} \\ g_{v_2} \\ g_{v_3} \\ g_{v_4} \\ g_{v_5} \end{bmatrix} = \begin{bmatrix} 0 \\ D\eta_x\tau_{xx} + D\eta_y\tau_{xy} + D\eta_z\tau_{xz} \\ D\eta_x\tau_{xy} + D\eta_y\tau_{yy} + D\eta_z\tau_{yz} \\ D\eta_x\tau_{xz} + D\eta_y\tau_{yz} + D\eta_z\tau_{zz} \\ ug_{v_2} + vg_{v_3} + wg_{v_4} + \dfrac{\gamma}{\gamma-1}\tilde{\mu}_e\left(c_4\dfrac{\partial T}{\partial\xi} + c_5\dfrac{\partial T}{\partial\eta} + c_6\dfrac{\partial T}{\partial\zeta}\right) \end{bmatrix}$$

$$\boldsymbol{H}_v = \begin{bmatrix} h_{v_1} \\ h_{v_2} \\ h_{v_3} \\ h_{v_4} \\ h_{v_5} \end{bmatrix} = \begin{bmatrix} 0 \\ D\zeta_x\tau_{xx} + D\zeta_y\tau_{xy} + D\zeta_z\tau_{xz} \\ D\zeta_x\tau_{xy} + D\zeta_y\tau_{yy} + D\zeta_z\tau_{yz} \\ D\zeta_x\tau_{xz} + D\zeta_y\tau_{yz} + D\zeta_z\tau_{zz} \\ uh_{v_2} + vh_{v_3} + wh_{v_4} + \dfrac{\gamma}{\gamma-1}\tilde{\mu}_e\left(c_7\dfrac{\partial T}{\partial\xi} + c_8\dfrac{\partial T}{\partial\eta} + c_9\dfrac{\partial T}{\partial\zeta}\right) \end{bmatrix}$$

where

$$c_1 = D(\xi_x^2 + \xi_y^2 + \xi_z^2) \qquad \tau_{xx} = \frac{2}{3}\tilde{\mu}\left(2\frac{\partial u}{\partial x} - \frac{\partial v}{\partial y} - \frac{\partial w}{\partial z}\right)$$

$$c_2 = D(\xi_x\eta_x + \xi_y\eta_y + \xi_z\eta_z) \qquad \tau_{xy} = \tilde{\mu}\left(\frac{\partial u}{\partial y} + \frac{\partial v}{\partial x}\right)$$

$$c_3 = D(\xi_x\zeta_x + \xi_y\zeta_y + \xi_z\zeta_z) \qquad \tau_{xz} = \tilde{\mu}\left(\frac{\partial u}{\partial z} + \frac{\partial w}{\partial x}\right)$$

$$c_4 = D(\xi_x\eta_x + \xi_y\eta_y + \xi_z\eta_z) \qquad \tau_{yy} = \frac{2}{3}\tilde{\mu}\left(2\frac{\partial v}{\partial y} - \frac{\partial u}{\partial x} - \frac{\partial w}{\partial z}\right)$$

$$c_5 = D(\eta_x^2 + \eta_y^2 + \eta_z^2) \qquad \tau_{yz} = \tilde{\mu}\left(\frac{\partial v}{\partial z} + \frac{\partial w}{\partial y}\right)$$

$$c_6 = D(\eta_x\zeta_x + \eta_y\zeta_y + \eta_z\zeta_z) \qquad \tau_{zz} = \frac{2}{3}\tilde{\mu}\left(2\frac{\partial w}{\partial z} - \frac{\partial u}{\partial x} - \frac{\partial v}{\partial y}\right)$$

$$c_7 = D(\xi_x\zeta_x + \xi_y\zeta_y + \xi_z\zeta_z)$$

$$c_8 = D(\eta_x\zeta_x + \eta_y\zeta_y + \eta_z\zeta_z) \qquad \tilde{\mu} = \mu_l + \mu_t$$

$$c_9 = D(\zeta_x^2 + \zeta_y^2 + \zeta_z^2) \qquad \tilde{\mu}_e = \mu_l/Pr_l + \mu_t/Pr_t$$

and ρ, P, and T are the fluid density, pressure, and temperature; and E is the total energy per unit volume. $Pr_l = 0.72$ is the laminar Prandtl number, $Pr_t = 0.90$ is the turbulent Prandtl number, μ_l is the laminar viscosity found from Sutherland's Law, and μ_t is the turbulent viscosity obtained from the $k-\varepsilon$ turbulence model. The total energy and pressure of a calorically perfect gas are related through the equation of state:

$$P = (\gamma - 1)\left(E - \rho\frac{\boldsymbol{v}\cdot\boldsymbol{v}}{2}\right)$$

where $\gamma = 1.4$ is the ratio of specific heat capacities.

The eddy viscosity μ_t, required by the Reynolds-averaged Navier-Stokes equations, is modeled as:

$$\mu_t = C_\mu(k^2/\varepsilon) \tag{2}$$

where k is the turbulence kinetic energy, ε is the dissipation rate of the turbulence kinetic energy, and C_μ is a scalar constant for isotropic turbulence. The basic high-Reynolds-number $k-\varepsilon$ turbulence model of Launder and Spalding[5] is used, together with a standard wall function, to calculate these turbulent viscosities. The standard $k-\varepsilon$ model is chosen because of its computational efficiency and ability to model accurately a variety of different flows (Avva, Kline, and Ferzinger[6]). Although far from being a universal turbulence model, the high-Reynolds-number $k-\varepsilon$ model was chosen over the more widely used algebraic models for the following reasons:

1) wakes are captured without having to be located and treated uniquely,

2) it is less sensitive to skewed or nonorthogonal mesh cells near solid walls, and

3) the wall function treatment, which makes no attempt to resolve the flow within the laminar viscous sublayer, requires fewer mesh cells.

The $k-\varepsilon$ equations can be written:

$$\frac{\partial \boldsymbol{W}_{k\varepsilon}}{\partial t} + \frac{\partial \boldsymbol{F}_{k\varepsilon}}{\partial\xi} + \frac{\partial \boldsymbol{G}_{k\varepsilon}}{\partial\eta} + \frac{\partial \boldsymbol{H}_{k\varepsilon}}{\partial\zeta} = \boldsymbol{S}_{k\varepsilon} \tag{3}$$

where

$$\boldsymbol{W}_{k\varepsilon} = \begin{pmatrix} \rho Dk \\ \rho D\varepsilon \end{pmatrix} \qquad \boldsymbol{S}_{k\varepsilon} = \begin{pmatrix} s_1 \\ s_2 \end{pmatrix}$$

$$\boldsymbol{F}_{k\varepsilon} = \begin{bmatrix} \rho DUk - \mu_k\left(c_1\dfrac{\partial k}{\partial\xi} + c_2\dfrac{\partial k}{\partial\eta} + c_3\dfrac{\partial k}{\partial\zeta}\right) \\ \rho DU\varepsilon - \mu_\varepsilon\left(c_1\dfrac{\partial \varepsilon}{\delta\xi} + c_2\dfrac{\partial \varepsilon}{\partial\eta} + c_3\dfrac{\partial \varepsilon}{\partial\zeta}\right) \end{bmatrix}$$

$$\boldsymbol{G}_{k\varepsilon} = \begin{bmatrix} \rho DVk - \mu_k\left(c_4\dfrac{\partial k}{\partial\xi} + c_5\dfrac{\partial k}{\partial\eta} + c_6\dfrac{\partial k}{\partial\zeta}\right) \\ \rho DV\varepsilon - \mu_\varepsilon\left(c_4\dfrac{\partial \varepsilon}{\partial\xi} + c_5\dfrac{\partial \varepsilon}{\partial\eta} + c_6\dfrac{\partial \varepsilon}{\partial\zeta}\right) \end{bmatrix}$$

$$\boldsymbol{H}_{k\varepsilon} = \begin{bmatrix} \rho DWk - \mu_k\left(c_7\dfrac{\partial k}{\partial\xi} + c_8\dfrac{\partial k}{\partial\eta} + c_9\dfrac{\partial k}{\partial\zeta}\right) \\ \rho DW\varepsilon - \mu_e\left(c_7\dfrac{\partial \varepsilon}{\partial\xi} + c_8\dfrac{\partial \varepsilon}{\partial\eta} + c_9\dfrac{\partial \varepsilon}{\partial\zeta}\right) \end{bmatrix}$$

and

$$s_1 = D(\Theta - \rho\varepsilon) \qquad \mu_k = \mu_l + \mu_t/\sigma_k$$

$$s_2 = D(t_1\Theta - t_2\rho\varepsilon)\varepsilon/k \qquad \mu_\varepsilon = \mu_l + \mu_t\sigma_\varepsilon$$

for which the production rate of the turbulence kinetic energy

is defined as

$$\Theta = \left\{2\mu_t \frac{\partial u}{\partial x} - \frac{2}{3}\left[\rho k + \mu_t\left(\frac{\partial u}{\partial x} + \frac{\partial v}{\partial y} + \frac{\partial w}{\partial z}\right)\right]\right\}\frac{\partial u}{\partial x} + \left\{2\mu_t \frac{\partial v}{\partial y} - \frac{2}{3}\left[\rho k + \mu_t\left(\frac{\partial u}{\partial x} + \frac{\partial v}{\partial y} + \frac{\partial w}{\partial z}\right)\right]\right\}\frac{\partial v}{\partial y} + \left\{2\mu_t \frac{\partial w}{\partial z} - \frac{2}{3}\left[\rho k + \mu_t\left(\frac{\partial u}{\partial x} + \frac{\partial v}{\partial y} + \frac{\partial w}{\partial z}\right)\right]\right\}\frac{\partial w}{\partial z} + \mu_t\left(\frac{\partial u}{\partial y} + \frac{\partial u}{\partial z} + \frac{\partial v}{\partial x} + \frac{\partial v}{\partial z} + \frac{\partial w}{\partial x} + \frac{\partial w}{\partial y}\right)^2$$

The turbulence modeling constants are chosen to be the standard Launder and Spalding[9] values of

$$C_\mu = 0.09 \quad t_1 = 1.44 \quad t_2 = 1.92 \quad \sigma_k = 1.0 \quad \sigma_\varepsilon = 1.3$$

and were never altered during the course of this work. (Isotropy is assumed since C_μ is a scalar constant rather than a nonconstant vector quantity.) The transformed Navier-Stokes and $k-\varepsilon$ equations are discretized by a finite-volume formulation that approximates the spatial differences as a net flux across the faces of each mesh cell. Global conservation and the admission of possible uniform flow solutions are insured by evaluating both the inviscid and viscous flux vectors on the faces of the boundary-conforming mesh cells. This procedure requires that the flow and $k-\varepsilon$ variables, viscous stresses, and flux-embedded geometric quantities be defined on the faces of the mesh cells during the flux evaluations, although it is the cell-averaged flow and $k-\varepsilon$ variables that are calculated during the time and spatial marching. The viscous stresses and geometric quantities are evaluated directly on the cell faces, while the flow and $k-\varepsilon$ variables are averaged over values found in adjacent cells. The unsteady equations can be discretized into an implicit approximation that, when written in a linearized delta form, produces a numerical scheme whose steady-state solutions are independent of the time step size used in the time marching. The computational effort required to construct this implicit approximation is kept at a minimum by treating only the inviscid fluxes. The delta form, produced by linearizing the changes in the inviscid flux vectors through a Taylor series expansion about a time level n, can be written for the flow equations as follows:

$$[I + \mu_i\,\Delta t(\delta_\xi A + \delta_\eta B + \delta_\zeta C)]\,\Delta \boldsymbol{W}^n_{ijk} = -\Delta t[\bar{\delta}_\xi(\boldsymbol{F} - \boldsymbol{F}_v) + \bar{\delta}_\eta(\boldsymbol{G} - \boldsymbol{G}_v) + \bar{\delta}_\zeta(\boldsymbol{H} - \boldsymbol{H}_v)]^n_{ijk} \tag{4}$$

where

$$\Delta \boldsymbol{W}^n = \boldsymbol{W}^{n+1} - \boldsymbol{W}^n$$

and Δt is the time step size; $0 \le \mu_i \le 1$ is a parameter governing the degree of implicitness; δ and $\bar{\delta}$ are cell- and face-centered central differences; I is the identity matrix; and A, B, and C are the inviscid flux Jacobian matrices relative to the vectors $\boldsymbol{F}$, $\boldsymbol{G}$, and $\boldsymbol{H}$. The implicit form of the $k-\varepsilon$ equations can be written as follows:

$$[I + \mu_i\,\Delta t(\delta_\xi A_{k\varepsilon} + \delta_\eta B_{k\varepsilon} + \delta_\zeta C_{k\varepsilon} - E_{k\varepsilon})]\,\Delta \boldsymbol{W}^n_{k\varepsilon}|_{ijk} = -\Delta t(\bar{\delta}_\xi \boldsymbol{F}_{k\varepsilon} + \bar{\delta}_\eta \boldsymbol{G}_{k\varepsilon} + \bar{\delta}_\zeta \boldsymbol{H}_{k\varepsilon} - \boldsymbol{S}_{k\varepsilon})^n_{ijk} \tag{5}$$

and

$$\Delta \boldsymbol{W}^n_{k\varepsilon} = \boldsymbol{W}^{n+1}_{k\varepsilon} - \boldsymbol{W}^n_{k\varepsilon}$$

where $A_{k\varepsilon}$, $B_{k\varepsilon}$, and $C_{k\varepsilon}$ are the inviscid flux Jacobian matrices relative to the inviscid terms found in the vectors $\boldsymbol{F}_{k\varepsilon}$, $\boldsymbol{G}_{k\varepsilon}$, and $\boldsymbol{H}_{k\varepsilon}$; and $E_{k\varepsilon}$ is the Jacobian matrix relative to the source vector $\boldsymbol{S}_{k\varepsilon}$.

Artificial Dissipation

The finite-volume formulation reduces to a central difference approximation on a uniform grid and therefore requires the addition of explicit artificial dissipation terms to suppress possible odd and even point oscillations and shock overshoots. Following the works of Jameson[7] and Pulliam,[8] fourth difference terms are added throughout the flowfield to prevent odd-even decoupling, while second difference terms are used to stabilize the flow calculation near shocks.

The conservatively added dissipative term is an adaptive nonlinear blend of second and fourth differences that acts to turn on the second and turn off the fourth difference terms near a shock. A local Mach number scaling, similar to the treatment suggested by Flores and Holst,[9] is included in these terms to prevent the addition of artificial dissipation to viscous-dominated flow regions near solid walls. The dissipative terms added to the flow equations are of the form:

$$\boldsymbol{T}_i = -\delta_\xi M_l \phi^{(2)} D \delta_\xi \frac{1}{D}\boldsymbol{W}_i + \delta_\xi M_l \phi^{(4)} D \delta_{\xi\xi\xi}\frac{1}{D}\boldsymbol{W}_i \tag{6}$$

where the shock sensing term below:

$$v_i = \frac{|P_{i+1} - 2P_i + P_{i-1}|}{P_{i+1} + 2P_i + P_{i-1}}$$

is used to define the following nonlinear scaling factors:

$$\phi^{(2)}_{i+1/2} = \frac{\chi^{(2)}}{\Delta t'_{i+1/2}}\max(v_{i+2}, v_{i+1}, v_i, v_{i-1})$$

$$\phi^{(4)}_{i+1/2} = \max\left(0, \frac{\chi^{(4)}}{\Delta t'_{i+1/2}} - k^{(2)}_{i+1/2}\right)$$

where $\chi^{(2)}$ and $\chi^{(4)}$ are scalar constants and $\Delta t'$ is a one-dimensional unit Courant number time step scaling factor. M_l is the local Mach number scaling that is normalized by the inflow Mach number and limited to a maximum value of unity. Dissipative terms are also added to the $k-\varepsilon$ equations and are second difference terms of the form:

$$\boldsymbol{T}_{k\varepsilon}|_i = -\delta_\xi M_l \phi^{(k\varepsilon)} D \delta_\xi \frac{1}{D}\boldsymbol{W}_{k\varepsilon}|_i \tag{7}$$

where

$$\phi^{(k\varepsilon)}_{i+1/2} = \frac{\chi^{(k\varepsilon)}}{\Delta t'_{i+1/2}}$$

and $\chi^{(k\varepsilon)}$ is a scalar constant.

LU Approximate Factorization

The block-banded implicit delta operator is factored into two block triangular operators to circumvent the considerable amounts of CPU time and temporary storage needed to solve this unfactored implicit approximation. The LU factorization, which is based on one-sided, implicit, spatial differences, can be written for the flow equations as:

$$[I + \mu_i\,\Delta t(\delta_\xi^- A_1 + \delta_\eta^- B_1 + \delta_\zeta^- C_1)] \cdot [I + \mu_i\,\Delta t(\delta_\xi^+ A_2 + \delta_\eta^+ B_2 + \delta_\zeta^+ C_2)]\,\Delta \boldsymbol{W}^n_{ijk} = -\Delta t(\bar{\delta}_\xi(\boldsymbol{F} - \boldsymbol{F}_v) + \bar{\delta}_\eta(\boldsymbol{G} - \boldsymbol{G}_v) + \delta_\zeta(\boldsymbol{H} - \boldsymbol{H}_v) + \boldsymbol{T})^n_{ijk} \tag{8}$$

and for the $k-\varepsilon$ equations as follows:

$$[I + \mu_i\,\Delta t(\delta_\xi^- A_{k\varepsilon_1} + \delta_\eta^- B_{k\varepsilon_1} + \delta_\zeta^- C_{k\varepsilon_1} - E_{k\varepsilon_1})] \cdot [I + \mu_i\,\Delta t(\delta_\xi^+ A_{k\varepsilon_2} + \delta_\eta^+ B_{k\varepsilon_2} + \delta_\zeta^+ C_{k\varepsilon_2} - E_{k\varepsilon_2})]\,\Delta \boldsymbol{W}_{k\varepsilon}|^n_{ijk} = -\Delta t(\bar{\delta}_\xi \boldsymbol{F}_{k\varepsilon} + \delta_\eta \boldsymbol{G}_{k\varepsilon} + \delta_\zeta \boldsymbol{H}_{k\varepsilon} + \boldsymbol{T}_{k\varepsilon} - \boldsymbol{S}_{k\varepsilon})^n_{ijk} \tag{9}$$

where δ^+ and δ^- are cell-centered forward and backward first differences, and the inviscid flux Jacobian matrices are split and reconstructed as:

$$A_1 = (A + \beta|A|I)/2 \qquad A_2 = (A - \beta|A|I)/2$$

$$A_{k\varepsilon_1} = (A_{k\varepsilon} + \beta|A|I)/2 \qquad A_{k\varepsilon_2} = (A_{k\varepsilon} - \beta|A|I)/2$$

where

$$|A| = \max(|\lambda_A|)$$

is the maximum absolute-valued eigenvalue of the Jacobian matrix A, $\beta \approx 1$ is a scalar constant governing the amount of implicit dissipation produced by the matrix reconstructions, and I is the identity matrix. This splitting is chosen to insure a nonsingular diagonal inversion and is similar to the Jameson and Turkel[10] splitting that produces diagonally dominant implicit factors for each matrix inversion in every mesh cell.[11] This LU factorization requires the solution of two block triangular operators, each of which, through back substitution, can be reduced to simple 5×5 matrix systems at every mesh cell. These reduced systems can be written as follows:

Lower Sweep

$$[I + \mu_i \Delta t(A_1 + B_1 + C_1)]\, \Delta \boldsymbol{Y}^n_{ijk}$$

$$= -\Delta t(\delta_\xi(\boldsymbol{F} - \boldsymbol{F}_v) + \delta_\eta(\boldsymbol{G} - \boldsymbol{G}_v) + \delta_\zeta(\boldsymbol{H} - \boldsymbol{H}_v) + \boldsymbol{T})^n_{ijk}$$

$$+ \mu_i \Delta t(A_1\, \Delta \boldsymbol{Y}^n_{i-1,j,k} + B_1\, \Delta \boldsymbol{Y}^n_{i,j-1,k} + C_1\, \Delta \boldsymbol{Y}^n_{i,j,k-1}) \quad (10)$$

Upper Sweep

$$[I - \mu_i \Delta t(A_2 + B_2 + C_2)]\, \Delta \boldsymbol{W}^n_{ijk}$$

$$= \Delta \boldsymbol{Y}^n_{ijk} - \mu_i \Delta t(A_2\, \Delta \boldsymbol{W}^n_{i+1,j,k} + B_2\, \Delta \boldsymbol{W}^n_{i,j+1,k}$$

$$+ C_2\, \Delta \boldsymbol{W}^n_{i,j,k+1}) \quad (11)$$

A similar analysis for the k–ε equations can be used to write the following 2×2 matrix equations:

Lower Sweep

$$[I + \mu_i \Delta t(A_{k\varepsilon_1} + B_{k\varepsilon_1} + C_{k\varepsilon_1} - E_{k\varepsilon_1})]\, \Delta \boldsymbol{Y}_{k\varepsilon}|^n_{ijk}$$

$$= -\Delta t(\delta_\xi \boldsymbol{F}_{k\varepsilon} + \delta_\eta \boldsymbol{G}_{k\varepsilon} + \delta_\zeta \boldsymbol{H}_{k\varepsilon} - E_{k\varepsilon} + \boldsymbol{T}_{k\varepsilon})^n_{ijk}$$

$$+ \mu_i \Delta t(A_{k\varepsilon_1}\, \Delta \boldsymbol{Y}_{k\varepsilon}|^n_{i-1,j,k} + B_{k\varepsilon_1}\, \Delta \boldsymbol{Y}_{k\varepsilon}|^n_{i,j-1,k}$$

$$+ C_{k\varepsilon_1}\, \Delta \boldsymbol{Y}_{k\varepsilon}|^n_{i,j,k-1}) \quad (12)$$

Upper Sweep

$$[I - \mu_i \Delta t(A_{k\varepsilon_2} + B_{k\varepsilon_2} + C_{k\varepsilon_2} - E_{k\varepsilon_2})]\, \Delta \boldsymbol{W}_{k\varepsilon}|^n_{ijk}$$

$$= \Delta \boldsymbol{Y}_{k\varepsilon}|^n_{ijk} - \mu_i \Delta t(A_{k\varepsilon_2}\, \Delta \boldsymbol{W}_{k\varepsilon}|^n_{i+1,j,k} + B_{k\varepsilon_2}\, \Delta \boldsymbol{W}_{k\varepsilon}|^n_{i,j+1,k}$$

$$+ C_{k\varepsilon_2}\, \Delta \boldsymbol{W}_{k\varepsilon}|^n_{i,j,k+1}) \quad (13)$$

Diagonally Inverted LU Factorization

The LU factorization of the k–ε equations produces simple 2×2 matrix systems that can be inverted algebraically, while the matrix systems associated with the flow equations are diagonally inverted using the similarity transformation[4] that produces the following diagonal matrix:

$$Q^{-1}(A + B + C)Q = \Lambda$$

having elements

$$\lambda_{11} = \lambda_{22} = \lambda_{33} = U + V + W$$

$$\lambda_{44} = U + V + W - c\sqrt{l_1^2 + l_2^2 + l_3^2}$$

$$\lambda_{55} = U + V + W + c\sqrt{l_1^2 + l_2^2 + l_3^2}$$

$$\lambda_{ij} = 0 \quad \text{when} \quad i \neq j$$

where

$$q^2 = u^2 + v^2 + w^2$$

$$l_1 = \xi_x + \eta_x + \zeta_x$$

$$l_2 = \xi_y + \eta_y + \zeta_y$$

$$l_3 = \xi_z + \eta_z + \zeta_z$$

and c is the local speed of sound. This similarity transformation, for a local time step defined as:

$$\Delta t = \frac{Cn}{(|A| + |B| + |C|)}$$

where Cn is the Courant number used in the time marching, can be used to transform the lower and upper sweeps into scalar equations with the following vector components ($m = 1,\ldots,5$)

Lower Sweep

$$(Q^{-1}\, \Delta \boldsymbol{Y}^n_{ijk})_m = \frac{\left(\begin{array}{l} -\Delta t Q^{-1}\{[\delta_\xi(\boldsymbol{F} - \boldsymbol{F}_v) + \delta_\eta(\boldsymbol{G} - \boldsymbol{G}_v) \\ \quad + \delta_\zeta(\boldsymbol{H} - \boldsymbol{H}_v) + \boldsymbol{T}]^n_{ijk} - \mu_i(A_1\, \Delta \boldsymbol{Y}^n_{i-1,j,k} \\ \quad + B_1\, \Delta \boldsymbol{Y}^n_{i,j-1,k} + C_1\, \Delta \boldsymbol{Y}^n_{i,j,k-1})\} \end{array}\right)_m}{[(1 + \mu_i \beta Cn/2)I + \mu\, \Delta t \Lambda/2]_m} \quad (14)$$

Upper Sweep

$$(Q^{-1}\, \Delta \boldsymbol{W}^n_{ijk})_m = \frac{\left(\begin{array}{l} Q^{-1}[\Delta \boldsymbol{Y}^n_{ijk} - \mu_i\, \Delta t(A_2\, \Delta \boldsymbol{W}^n_{i+1,j,k} \\ \quad + B_2\, \Delta \boldsymbol{W}^n_{i,j+1,k} + C_2\, \Delta \boldsymbol{W}^n_{i,j,k+1})] \end{array}\right)_m}{[(1 + \mu_i \beta Cn/2)I - \mu\, \Delta t \Lambda/2]_m} \quad (15)$$

and

$$\boldsymbol{W}^{n+1}_{ijk} = Q(Q^{-1}\, \Delta \boldsymbol{W}^n_{ijk}) + \boldsymbol{W}^n_{ijk}$$

These two steps can be then approximated by the even simpler systems:

Lower Sweep

$$(Q^{-1}\, \Delta \boldsymbol{Y}^n_{ijk})_m = \frac{\left(\begin{array}{l} -\Delta t\{Q^{-1}[\delta_\xi(\boldsymbol{F} - \boldsymbol{F}_v) + \delta_\eta(\boldsymbol{G} - \boldsymbol{G}_v) \\ \quad + \delta_\zeta(\boldsymbol{H} - \boldsymbol{H}_v) + \boldsymbol{T}]^n_{ijk} - \mu_i(\tilde{D}_{a_1} Q^{-1}\, \Delta \boldsymbol{Y}^n_{i-1,j,k} \\ \quad + \tilde{D}_{b_1} Q^{-1}\, \Delta \boldsymbol{Y}^n_{i,j-1,k} + \tilde{D}_{c_1} Q^{-1}\, \Delta \boldsymbol{Y}^n_{i,j,k-1})\} \end{array}\right)_m}{[(1 + \mu_i \beta Cn/2)I + \mu\, \Delta t \Lambda/2]_m} \quad (16)$$

Upper Sweep

$$(Q^{-1}\, \Delta \boldsymbol{W}^n_{ijk})_m = \frac{\left(\begin{array}{l} Q^{-1}\, \Delta \boldsymbol{Y}^n_{ijk} - \mu_i\, \Delta t(\tilde{D}_{a_2} Q^{-1}\, \Delta \boldsymbol{W}^n_{i+1,j,k} \\ \quad + \tilde{D}_{b_2} Q^{-1}\, \Delta \boldsymbol{W}^n_{i,j+1,k} \\ \quad + \tilde{D}_{c_2} Q^{-1}\, \Delta \boldsymbol{W}^n_{i,j,k+1}) \end{array}\right)_m}{[(1 + \mu_i \beta Cn/2)I - \mu\, \Delta t \Lambda/2]_m} \quad (17)$$

where $\tilde{D}_{a_1} = 0.5(\tilde{D}_a + \beta|A|I)$; $\tilde{D}_{a_2} = 0.5(\tilde{D}_a - \beta|A|I)$; and $\tilde{D}_a$ contains only the diagonal elements of the symmetric matrix $Q^{-1}AQ$ [i.e., $\tilde{d}_{a_{11}} = \tilde{d}_{a_{22}} = \tilde{d}_{a_{33}} = U$; $\tilde{d}_{a_{44}} = U + c(\xi_x l_1 + \xi_y l_2 + \xi_z l_3)$; and $\tilde{d}_{a_{55}} = U - c(\xi_x l_1 + \xi_y l_2 + \xi_z l_3)$, with similar terms for $\tilde{D}_{b_1}$, $\tilde{D}_{b_2}$, $\tilde{D}_{c_1}$, and $\tilde{D}_{c_2}$)]. The solution of these scalar equations requires less computational effort than the original matrix equations and significantly increases the computational efficiency of the LU factorization.[4]

Initial and Boundary Conditions

Initial conditions are needed to start the calculations and are chosen to be a uniform flowfield based on an initial guess of the upstream flow.

During the residual calculation, a no-slip condition is enforced along the solid boundaries. This treatment requires that only pressure needs to be specified along solid boundaries and is obtained from a three-dimensional interpretation of the normal momentum analysis developed by Rizzi.[12] For a solid boundary aligned with an $\eta-\zeta$ plane, the normal momentum analysis requires that the following equation be satisfied:

$$a_1 \frac{\partial P}{\partial \xi} + a_2 \frac{\partial P}{\partial \eta} + a_3 \frac{\partial P}{\partial \zeta} = 0 \tag{18}$$

where

$$a_1 = (D\xi_x)^2 + (D\xi_y)^2 + (D\xi_z)^2$$

$$a_2 = D^2\xi_x\eta_x + D^2\xi_y\eta_y + D^2\xi_z\eta_z$$

$$a_3 = D^2\xi_x\zeta_x + D^2\eta_y\zeta_y + D^2\xi_z\zeta_z$$

For a steady subsonic inflow boundary, total pressure, total temperature, and two flow angles are specified while a one-dimensional Riemann invariant

$$R = q - \frac{2c}{\gamma - 1}$$

is extrapolated from the interior flowfield (similar to the treatment used by Chima[13]). An inlet boundary-layer profile is specified by fixing a constant inlet total temperature and varying the inlet total pressure with a power law velocity profile.[14] For steady subsonic outflow, the specified boundary condition is a nonreflective treatment, based on the work of Rudy and Strikwerda,[15] that attempts to minimize unwanted reflected waves from the outflow boundary. Static pressures are obtained from a radial momentum analysis

$$\frac{1}{\rho}\frac{\partial P}{\partial r} = \frac{U_\theta^2}{r}$$

(where r is radial distance and U_θ is tangential velocity) and then coupled with the incoming compatibility relation to produce a nonreflective boundary condition

$$\frac{\partial P}{\partial t} - \frac{\rho \tilde{C}}{\zeta_z}\frac{\partial w}{\partial t} + \alpha(P - P_{\text{ref}}) = 0 \tag{19}$$

where

$$\tilde{C} = c\sqrt{\zeta_x^2 + \zeta_y^2 + \zeta_z^2}$$

Here P_{ref} is the static pressure obtained from the radial momentum equation and $\alpha \approx 1$ is a scalar constant.

The initial conditions used to start the $k-\varepsilon$ calculations are a uniform field based on the inflow $k-\varepsilon$ boundary conditions. A 2% turbulence intensity is assumed upstream and is used to produce the following inflow boundary conditions:

$$k = 1.5(0.02Q)^2 \qquad \varepsilon = k^{3/2}/0.01 \tag{20}$$

where Q is the mean upstream speed. A zeroth-order extrapolation of the $k-\varepsilon$ values is used to specify conditions at the outflow boundary.

The turbulent viscosity is set to zero along solid walls while a standard wall function[5] is used to evaluate the $k-\varepsilon$ variables in cells immediately adjacent to solid walls. The wall function takes the form

$$\frac{U_1}{U_\tau} = \frac{\ell n(E_c Y^+)}{\kappa_{vk}} \tag{21}$$

where

$$Y^+ = \frac{\rho_1 U_\tau y_1}{\mu_1}$$

and ρ_1, μ_1, Y_1, and U_1 are the fluid density, laminar viscosity, distance, and tangential velocity found in the first mesh cell away from a solid wall. $\kappa_{vk} = 0.41$ is the von Karman constant and E_c is a wall roughness constant that has a value of $E_c = 9$ for smooth walls. The wall function is solved by a Newton-Raphson iterative method, and the resulting friction velocity U_τ is used to evaluate the $k-\varepsilon$ variables as follows

$$k_1 = \frac{U_\tau^2}{\sqrt{C_\mu}} \qquad \varepsilon_1 = \frac{U_\tau^3}{\kappa_{vk} y_1} \tag{22}$$

Steady-State Calculations

The calculation of steady-state solutions is made more efficient by using local time-stepping and the multigrid method.

Local time stepping is used to optimize the time step throughout the flowfield. A locally varying time-step size, based on a constant Courant number, is used to create a warped time integration that can accelerate the calculation to a steady state without affecting the steady-state solution. These time steps are defined identically for both the flow and $k-\varepsilon$ equations, although the value of the Courant numbers used in their evaluation may vary. Given the spectral radii of the flow and $k-\varepsilon$ equations

$$\rho_f \approx |U + V + W| + c\sqrt{l_1^2 + l_2^2 + l_3^2}$$

$$\rho_{k\varepsilon} \approx |U + V + W|$$

the following time steps can be defined

$$\Delta t_f = \frac{C_n}{\rho_f} \qquad \Delta t_{k\varepsilon} = \frac{C_n}{\rho_{k\varepsilon}}$$

For a given Courant number, the time step for the flow equations would be significantly smaller than that of the $k-\varepsilon$ equations. To insure that these two time steps are comparable in size, two Courant numbers, different in magnitude, would need to be used.

The multigrid method is incorporated into the diagonally inverted LU scheme to accelerate the removal of low-frequency errors from the flow solution and thus increase the efficiency of the time-marching procedure. Following the work of Jameson,[16] the flow solver is used to smooth out high-frequency errors resolvable on any current grid level (h), while the multigrid method is used to eliminate low-frequency errors through a sequence of flow calculations on coarser grids ($2h$,$4h$,$8h$,...). The multigrid sequencing used is a four-level W-cycle, where coarse grid boundary conditions are identical to those used on the fine grid with the exception of the inflow/outflow conditions, which are updated only on the fine grids. The Reynolds-averaged Navier-Stokes equations are solved on the finest grid while only the Euler fluxes are evaluated on the coarse grids. Coarse grid residuals are kept

smooth by adding only a constant coefficient second difference artificial dissipation term (the nonlinear blended terms are used only on the fine grid). This treatment attempts to limit the amount of high-frequency errors reintroduced into the flowfield by the upward interpolation of the coarse corrections. The flow solver, in this case the diagonally inverted LU scheme, is invoked only once on each grid level and only before transferring the flowfield to the respective coarse grid. The multigrid cycle defined above requires approximately 1.32 work units of computational effort, where work units are normalized by a single Navier-Stokes calculation on the finest grid. The $k-\varepsilon$ equations are solved only on the finest grid and are not accelerated with the multigrid method. Preliminary attempts at multigridding the $k-\varepsilon$ equations proved to be less efficient than simply solving these equations only on the finest grid. Since it is the time asymptote and not the solution at any current time step that is ultimately required, there seems to be little reason to multigrid the turbulence model between each fine grid flow calculation.

Results

Numerical results are presented to illustrate the diagonally inverted LU scheme's ability to calculate three-dimensional compressible viscous flows and the convergence acceleration produced by the multigrid method.

Turbomachinery calculations were performed on H-type grids consisting of 96 × 24 × 24 mesh cells in the throughflow, blade-to-blade, and radial directions, respectively. These grids were generated using a modified version of the grids about airfoils using Poisson's Equation (GRAPE) code[17] originally developed by Sorenson.[18] All calculations were performed on a CRAY X-MP, where a calculation consisting of 211 work units required approximately 1.5 million words of memory and 40 min of CPU time.

The test case used to evaluate the LU scheme is the Annular Cascade designed and extensively tested at NASA Lewis.[19,20] The computational grid shown in Fig. 1 is based on the full annular ring of 36 core turbine stator vanes. The geometry is a 38.10 mm high, untwisted blade of constant profile with an axial chord of 38.23 mm. The stator has a tip diameter of 508 mm and a 0.85 hub-to-tip radius ratio. Mesh cells found immediately adjacent to solid walls are centered at distances 0.002 of an axial chord away, which correspond to a value of $Y^+ \approx 60$ for the following flow calculations.

Experimental test conditions of ambient axial inflow and a 0.65 hub-static to inlet-total pressure ratio produce a flowfield with mean radius inlet and exit critical velocity ratios of 0.231 and 0.778, respectively. To match the upstream flow conditions (an inflow Mach number of 0.211), the calculations were run with a 0.665 hub-static to inlet-total pressure ratio.

Figure 2 shows the convergence history of a single-grid calculation where a drop of only two and a half orders of magnitude in the residual of the continuity equation was produced after 400 work units. A further reduction of the residual would require significantly more iterations since a "flattening out" of the convergence rate occurs after 300 work units.

The convergence history of the multigrid calculation is shown in Fig. 3 where a significant amount of acceleration can be observed. A residual drop of approximately four and a half orders of magnitude is produced within 400 work units and with no major "flattening out" of the convergence rate. A Courant number of six was used in the solution of the flow equations, while a Courant number of four was used in the $k-\varepsilon$ equations (no attempt to optimize these numbers was made).

The resulting flowfield is fully subsonic and is compared with experimental data at three spanwise positions. Figures 4, 5, and 6 compare the calculated blade surface static pressure distributions (normalized by inlet total pressure) at 13.3, 50, and 86.7% span with the experimental data prouced by

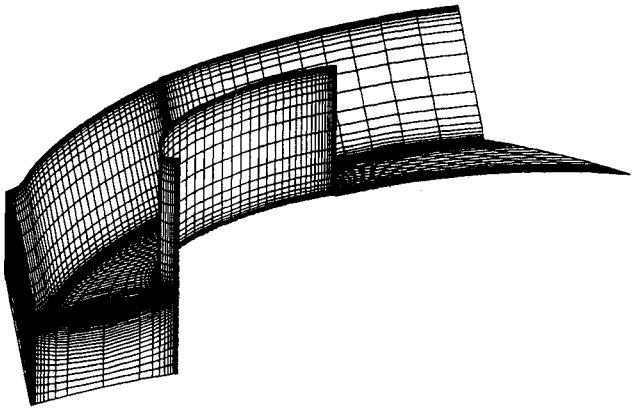

Fig. 1 Computational grid for the Annular Cascade.

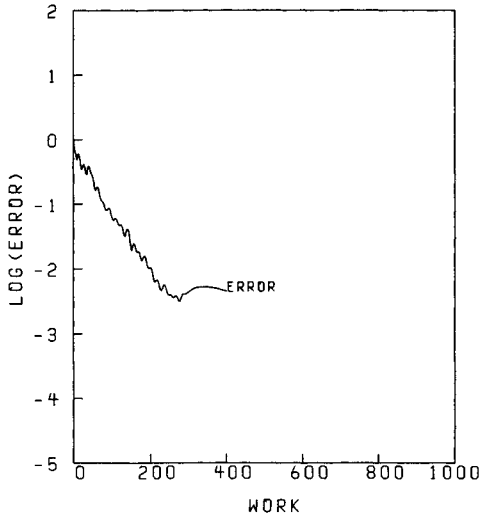

P.R. 0.6650 ANGY 90.00
ROT. 0.000 ANGZ 0.00
RES1 0.169E 01 RES2 0.760E-02
WORK 400.00 C.N. 6.0 RATE 0.9866

Fig. 2 Convergence history for the single-grid calculation.

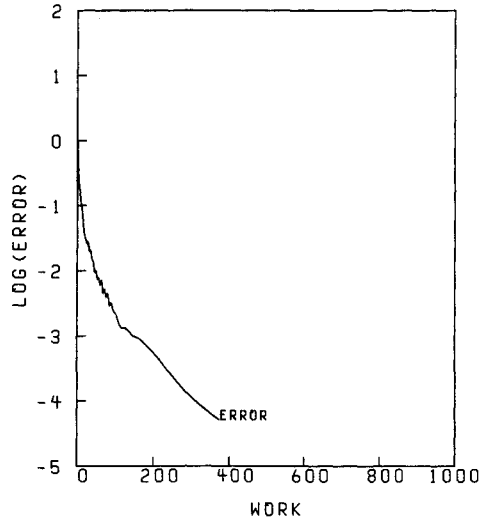

P.R. 0.6650 ANGY 90.00
ROT. 0.000 ANGZ 0.00
RES1 0.169E 01 RES2 0.871E-04
WORK 373.07 C.N. 6.0 RATE 0.9739

Fig. 3 Convergence history for the multigrid calculation.

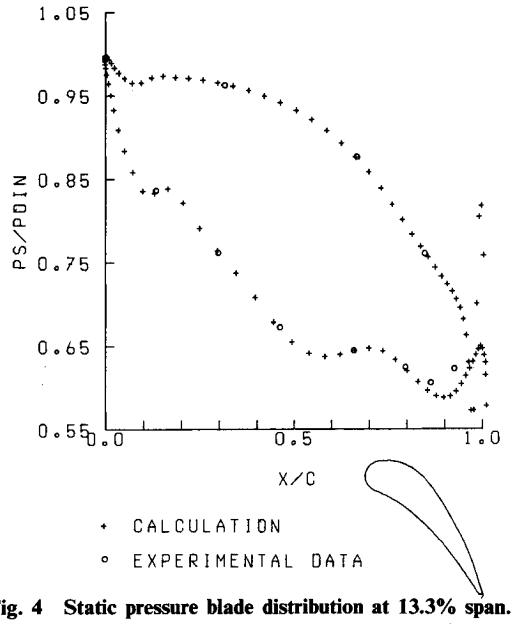

Fig. 4 Static pressure blade distribution at 13.3% span.

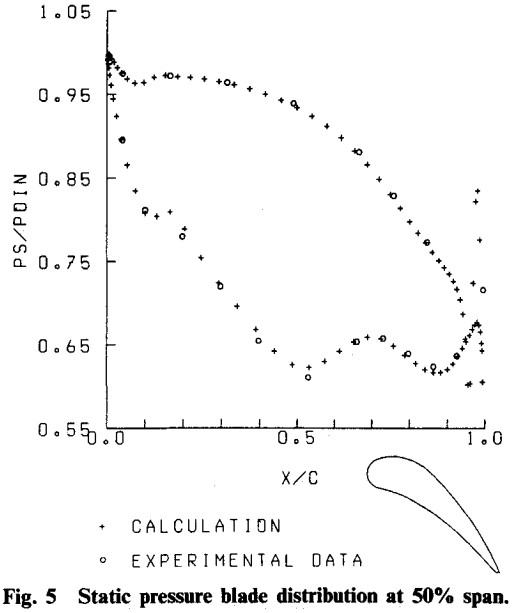

Fig. 5 Static pressure blade distribution at 50% span.

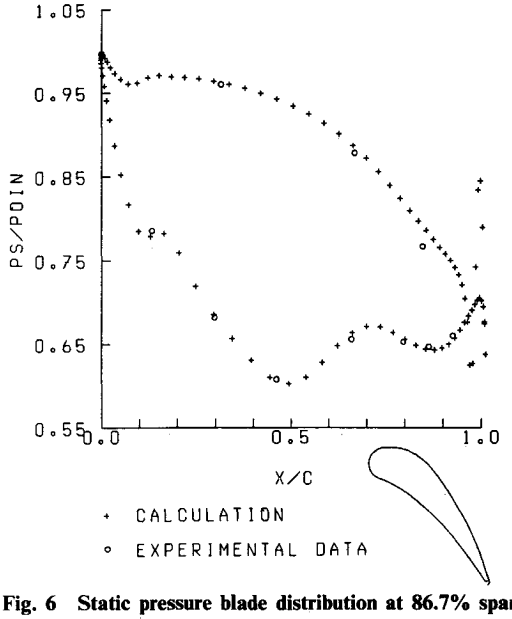

Fig. 6 Static pressure blade distribution at 86.7% span.

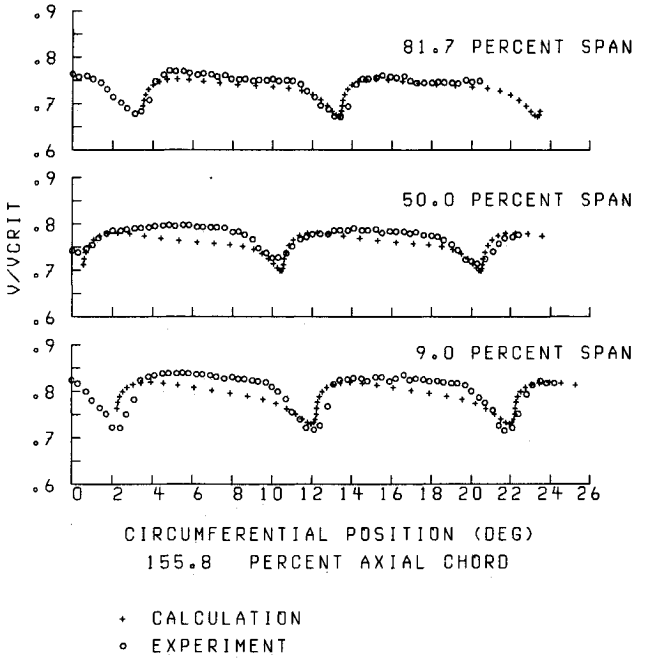

Fig. 7 Critical velocity ratio at 9, 50, and 82% span and 156% axial chord.

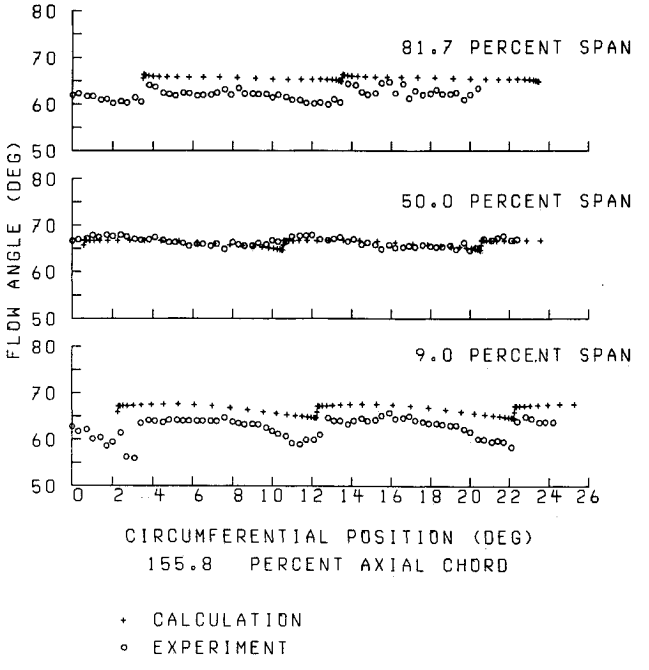

Fig. 8 Flow angle at 9, 50, and 82% span and 156% axial chord.

Goldman and Seasholtz.[20] The trailing-edge flow is not captured smoothly (as expected) due to the bluntness of the blade's trailing edge but the overall results agree well with the experimental data. This agreement is most significant near the uncovered portion of the blade's suction surface, where an inadequate turbulence model can greatly affect the accuracy of the flow calculation. A laminar calculation will separate in this region while an algebraic turbulence model may not be able to resolve all the subtleties of the flowfield.[14]

Figure 7 shows the critical velocity ratio distributions along the 9, 50, and 81.7 percent radial span planes at the 155.8 percent axial chord location. The agreement between the computational and experimental results is extremely good and increases as one moves away from the hub and toward the tip region. This behavior may be due to the hub secondary flow

and the nonisotropic turbulence found within this region. In general, the flow calculation captures the viscous wake effects and agrees well with the slightly nonperiodic experimental data.

Figure 8 shows the flow angle comparisons at the three previously defined radial locations. The computational results compare extremely well with the experimental data at midspan but deviate from the experimental data as one moves away from this plane and toward the hub and tip regions. This result is due to the underprediction of the boundary layer thicknesses and is not unexpected since the $k-\varepsilon$ model assumes fully turbulent flow and a transition model has not been incorporated into the calculation.

Overall the numerical calculations compare well with the experimental data and demonstrate the scheme's ability to calculate complex flows.

Conclusion

A diagonally inverted LU implicit multigrid scheme has been developed for the three-dimensional Reynolds-averaged Navier-Stokes equations where turbulent viscosities are calculated from a two-equation $k-\varepsilon$ turbulence model. Results illustrate both the scheme's ability to calculate complex three-dimensional compressible flows and the convergence acceleration produced by the multigrid method.

Acknowledgments

It is with pleasure that I acknowledge the numerous conversations held throughout the course of this work with K. R. Kirtley and R. V. Chima. I am also grateful to D. A. Caughey for suggesting the spectral-radius/time-step analysis of the flow and $k-\varepsilon$ equations.

References

[1]Pulliam, T. H., and Steger, J. L., "Implicit Finite-Difference Simulations of Three-Dimensional Compressible Flow," *AIAA Journal*, Vol. 18, February 1980, pp. 159–167.

[2]Chaussee, D. S., and Pulliam, T. H., "Two-Dimensional Inlet Simulation using a Diagonal Implicit Algorithm," *AIAA Journal*, Vol. 19, February 1981, pp. 153–159.

[3]Jayaram, M., and Jameson, A., "Multigrid Solution of the Navier-Stokes Equations for Flow over Wings," AIAA Paper 88-705, 26th Aerospace Sciences Meeting, Reno, Nevada, January 1988.

[4]Yokota, J. W., Caughey, D. A., and Chima, R. V., "A Diagonally Inverted LU Implicit Multigrid Scheme," *Proceedings of the First National Fluid Dynamics Congress*, Part 1, AIAA, Washington DC, July 1988, pp. 104–111.

[5]Launder, B. E., and Spalding, D. B., "The Numerical Computation of Turbulent Flows," *Computer Methods in Applied Mechanics and Engineering*, Vol. 3, March 1974, pp. 269–289.

[6]Avva, R. K., Kline, S. J., and Ferzinger, J. H., "Computation of Turbulent Flow over a Backward-Facing Step-Zonal Approach," AIAA Paper 88-611, 26th Aerospace Sciences Meeting, Reno, Nevada, January 1988.

[7]Jameson, A., "Transonic Flow Calculations for Aircraft," *Lecture Notes in Mathematics*, edited by F. Brezzi, Vol. 1127, Springer-Verlag, New York, 1985, pp. 156–242.

[8]Pulliam, T. H., "Artificial Dissipation Models for the Euler Equations," AIAA Paper 85-0438, 23rd Aerospace Sciences Meeting, Reno, Nevada, January 1985.

[9]Flores, J., and Holst, T. L., "Numerical Solution of the Navier-Stokes Equations for Complex Configurations," *CFD for Aerospace Problems: Methods and Codes*, edited by K. C. Reddy and J. Steinhoff, University of Tennessee Space Institute Workshop, UTSI Publication No. E02-4005 013-88, March 1988.

[10]Jameson, A., and Turkel, E., "Implicit Schemes and LU Decompositions," *Mathematics of Computation*, Vol. 37, October 1981, pp. 385–397.

[11]Yokota, J. W., and Caughey, D. A., "An L-U Implicit Multigrid Algorithm for the Three-Dimensional Euler Equations," AIAA Paper 87-0453, 25th Aerospace Sciences Meeting, Reno, Nevada, January 1987.

[12]Rizzi, A., "Numerical Implementation of the Solid Body Boundary Conditions for the Euler Equations," *Zeitschrift fuer Angewandte Mathematik und Mechanik*, Vol. 58, 1978, pp. 301–304.

[13]Chima, R. V., "Analysis of Inviscid and Viscous Flows in Cascades with an Explicit Multi-Grid Algorithm," NASA TM-83636, 1984.

[14]Chima, R. V., and Yokota, J. W., "Numerical Analysis of Three-Dimensional Viscous Internal Flows," *Proceedings of the First National Fluid Dynamics Congress*, Part 1, AIAA, Washington DC, July 1988, pp. 17–24.

[15]Rudy, D. H., and Strikwerda, J. C., "A Nonreflecting Outflow Boundary Condition for Subsonic Navier-Stokes Calculations," *Journal of Computational Physics*, Vol. 36, June 1980, pp. 55–70.

[16]Jameson, A., "Solution of the Euler Equations for Two-Dimensional Transonic Flows by a Multigrid Method," Mechanical and Aerospace Engineering Report 1613, Princeton University, 1983.

[17]Smith, W. A., "Modified Grape Code," Sibley School of Mechanical and Aerospace Engineering Fluid Dynamics and Aerodynamics Report 87-10, Cornell University, Ithaca, NY, June 1987.

[18]Sorenson, R., "A Computer Program to Generate Two Dimensional Grids About Airfoils and Other Shapes by the use of the Poisson's Equation," NASA TM-81198, 1980.

[19]Goldman, L. J., and McLallin, K. L., "Cold-Air Annular Cascade Investigation of Aerodynamic Performance of Core-Engine-Cooled Turbine Vanes. I: Solid-Vane Performance and Facility Description," NASA TM-X-3224, 1975.

[20]Goldman, L. J., and Seasholtz, R. G., "Laser Anemometer Measurements in an Annular Cascade of Core Turbine Vanes and Comparison with Theory," NASA TP-2018, 1982.